Structural and mechanical properties of nanostructured tungsten oxide thin films

M. M. Hasan*[1], A. S. M. A. Haseeb[2] and H. H. Masjuki[2]

This study presents structural and mechanical properties of WO_3 thin films deposited on glass substrates at different temperatures by radio frequency reactive magnetron sputtering. WO_3 films deposited at temperatures up to 200°C are found as amorphous, but crystalline at 300 and 400°C. Chemical analysis reveals the overstoichiometry of the films. The diffusion of sodium ions from glass substrates occurs at higher temperatures. The adhesion critical loads of WO_3 films deposited at room temperature and at 200, 300 and 400°C are found to be 670, 990, 1080 and 830 mN respectively using microscratch tests with a 25 μm probe. Scratch hardness increases with the rise of temperature. The depth of penetration and wear track width decrease with temperature, indicating an improved penetration and wear resistance at temperatures up to 300°C. Scanning electron microscopy images reveal that the coatings fail due to wedge and recovery spallation during scratch and wear tests respectively.

Keywords: Structure, Morphology, Adhesion, Diffusion

Introduction

Tungsten trioxide (WO_3) is a wide band gap metal oxide semiconductor having outstanding properties for a variety of applications including electrochromic materials[1–6] and gas sensors.[7,8] WO_3 films also possess hydrophilic,[9] gasochromic[10] and photochromic properties.[11] Tungsten trioxide is one of the most widely studied electrochromic materials used as films. A promising application for these coatings is a switchable glazing for a smart window, which can save energy for air conditioning. Recently, WO_3 films have been considered for use as dielectric layers in multilayer heat mirror coatings on building and automotive glasses.[12] For most of these applications, thin films of WO_3 with nanometre thickness are usually deposited onto glass or polymeric substrates. A variety of conventional deposition methods have been used to prepare WO_3 films, such as dc or radio frequency (rf) magnetron sputtering,[4,5,13–19] sol–gel methods,[6,20,21] plasma spraying method,[7] chemical vapour deposition methods,[11,22,23] electron beam evaporation,[24,25] thermal evaporation[12,14] and hydrothermal methods.[2]

Sputter deposition technique is popular to produce adherent and uniform film over wide areas with better stoichiometric control. A number of studies on the deposition of WO_3 films by sputtering appear in the literature recently.[4,5,13–19] Most of the studies investigated electrochromic and gas sensing properties of WO_3 films. As the films are exposed to adverse environments, scratch and wear resistance play a significant role for their mechanical stability and durability. Few reports are available in the literature on the hardness, scratch resistance and wear behaviour of WO_3 films.[13–16,25–27] These studies attempted to evaluate mechanical and tribological properties of WO_3 films deposited mostly on metal substrates prepared by a variety of deposition techniques. Few reports are found to study tribological behaviour of WO_3 films deposited on metallic substrates using ball on plate or pin on disc tests.[14,25,26] These studies evaluated mechanical and/or tribological properties for tungsten oxide films of micrometre scale thickness using micro- and macroscale measurements. Maillé *et al.*[13] reported hardness of rf sputtered WO_3 films with a nanoscale thickness of 350 nm deposited on silicon substrates using nanoindentation technique. The adhesion critical loads were reported for WO_3 films deposited on high speed steel using dc reactive magnetron sputtering.[14–16] In these works, a conventional scratch testing machine with an indenter tip radius of 200 μm was employed to evaluate adhesion critical loads of micrometre scale films. Evaluation of mechanical properties of such thin films requires measurement techniques with control capability. Besides, a majority of the transparent functional tungsten oxide films are necessarily deposited on glass substrates as thin films. The investigations dealing with the mechanical properties of tungsten oxide thin films on glass substrates are scarce in the literature. From the past literatures, the mechanisms of wear and coating failures using SEM observations are also found scarce for tungsten oxide films.

Hence, in order to predict the durability of thin tungsten oxide films on glass substrate and a coating/substrate

[1]School of Applied Sciences and Technology, Shahjalal University of Science and Technology, Sylhet 3114, Bangladesh
[2]Department of Mechanical Engineering, Faculty of Engineering, University of Malaya, Kuala Lumpur 50603, Malaysia

*Corresponding author, email mmhasan92@yahoo.com

Published by Maney on behalf of the Institute
Received 27 April 2011; accepted 30 August 2012
DOI 10.1179/1743294412Y.0000000066

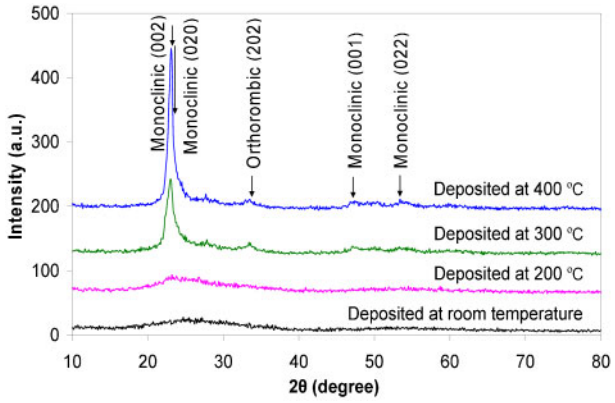

1 X-ray diffraction patterns of WO_3 films deposited at different substrate temperatures

system of great practical interest, it is important to have adequate data on their mechanical properties. In the present work, tungsten oxide thin films have been deposited on glass substrates by rf reactive magnetron sputtering at a constant sputtering pressure of 2 Pa. The main objective of this study is to evaluate mechanical properties such as scratch adhesion and wear resistance for WO_3 thin films deposited at different substrate temperatures on glass substrates. The effects of substrate temperatures on the structural properties have also been evaluated. In the present work, the mechanisms of wear and coating failures have been investigated under SEM as well.

Experimental

WO_3 thin films were deposited on microscope glass slides at room temperature and at 200, 300 and 400°C by rf reactive magnetron sputtering (without substrate bias) of tungsten target (purity of 99·95% and diameter of 100 mm). Before each deposition, the tungsten target was presputtered for 10 min in an argon atmosphere to remove oxide layers. The sputtering chamber was evacuated down to 5×10^{-4} Pa by a turbomolecular pump. The sputter deposition was performed in a mixture of 40 sccm of Ar (99·999%) and 20 sccm of O_2 (99·999%) atmosphere supplied as working and reactive gases respectively through an independent mass flow controller. During sputtering, the working pressure and rf power were kept constant at 2 Pa and 200 W respectively. Before deposition, the glass slides were sequentially cleaned in an ultrasonic bath with acetone and ethanol. Finally, they were rinsed with deionised water and dried with the blow of dry nitrogen (purity, 99·999%).

The phases present in the WO_3 films were analysed by an X-ray diffractometer (model D5000, Siemens) using Cu K_α radiations (λ=0·15406 nm) and operating at an accelerating voltage of 40 kV and an emission current of 40 mA. The crystallite size of the films was calculated using the Scherrer equation[28]

$$d=\frac{0{\cdot}89\lambda}{B\cos\theta} \quad (1)$$

where d is the crystallite size, λ is the wavelength of X-ray, B is the full width at half maximum of diffraction peak and θ is the diffraction angle. The chemical composition of samples was measured by means of an energy dispersive X-ray (EDX) analysis using an INCA 400 EDX energy analyser (Oxford Instruments) at an accelerating voltage of 10 kV. The thicknesses of the as deposited films at different temperatures were evaluated with the SEM cross-sectional images captured by a field emission SEM (FESEM) (FEI Quanta 200 FEG-SEM). The surface and cross-sectional morphologies of the as grown films were characterised under the FESEM.

The NanoTest platform of Micro Materials Ltd, UK, was used for the microscratch and wear testing. The system has a depth and load resolution better than 0·2 nm and 1 mN respectively. A 25 μm radius spherical diamond indenter (Rockwell sharp diamond) was used for the tests. The microscratch test was performed with a constant indenter velocity of 5 μm s^{-1}. An initial load of 1 mN was applied during the first 100 μm of the scratch, and the load was then increased to 1200 mN over a distance of 1400 μm at a fixed rate of 3 mN s^{-1}. Optical micrographs for the scratch tracks were captured under an optical microscope Olympus BX61, Japan. To observe the coating failure modes, the part of scratch tracks was investigated under a SEM (Philips XL30 SEM, Japan). The scratch hardness, which is a measure of the resistance of the material to normal penetration, is defined as[29]

$$SH=\frac{8N}{\pi d^2} \quad (2)$$

where SH is the scratch hardness in GPa, N is the applied normal force in N and d is the corresponding scratch width in μm. In this investigation, scratch hardness of the studied films is measured at three positions on the scratch tracks before the coating failure, and the average value was taken into consideration.

The procedure for wear tests involved a set of five topography scans and four wear scans at a constant velocity of 1 μm s^{-1} along the same surface on the films unidirectionally. In each topography scan including the first scan, the indenter moves at a constant load of 2 mN. In each wear scan, an initial load of 2 mN was applied during the first 200 μm, and then a constant load of 500 mN was abruptly applied for the further scan of 800 μm. Each wear scan is followed by a topography scan. The wear tracks were investigated under the SEM. The wear track width was measured at three different locations along the wear tracks of the studied films.

Results and discussion

Structural and morphological properties

Figure 1 shows the XRD patterns of WO_3 films deposited at different temperatures. The films deposited at lower temperatures, i.e. at room temperature and at 200°C, are observed to be amorphous. On the other hand, higher substrate temperatures of 300 and 400°C yield the mixed monoclinic and orthorhombic phases in WO_3 films with the predominance of former phase. The preferential orientation of the diffraction peak corresponding to the lattice reflection plane of (002) for monoclinic phase is clearly observable (Joint Committee on Powder Diffraction Standards card no. 431035). The peak at the 2θ range of 22·6 to 23·9° can be attributed to the combinations of two lattice planes of (002) and (020) for monoclinic phase. A weak peak of (202) for orthorhombic phase is also observable (Joint Committee

on Powder Diffraction Standards card no. 710131). Dimitrova and Gogova[22] observed amorphous structure in the WO_3 film deposited at 200°C by chemical vapour deposition. Their films on glass substrates showed crystalline phases at higher deposition temperatures of 300 and 400°C. Akl *et al.*[18] obtained preferentially oriented monoclinic structured films prepared by rf sputtering at a substrate temperature of 350°C. Using the Scherrer formula, the calculated crystallite sizes of the WO_3 films deposited at 300 and 400°C in the present study are found to be 9 and 13·5 nm respectively. Apparently, it shows an increase in crystallite size with the increase in substrate temperatures. The crystallite sizes obtained in the present study are in good agreement with the results found by Akl *et al.*[18] Wang *et al.*[19] reported that the crystallite size was found to increase from 30 to 45 nm with the increase in substrate temperature from 170 to 250°C for their rf sputtered WO_3 films at an elevated pressure of 4 Pa.

Table 1 shows the concentrations (at-%) of different elements from chemical analysis by EDX. Energy dispersive X-ray analysis indicates that the as grown film at room temperature contains mainly W and O. The absence of any silicon peak confirms that oxygen content found by EDX is not affected by the glass substrate. The film is observed to be overstoichiometric having the atomic ratio (O/W) of 3·56 as shown in Table 1. In general, the overstoichiometry of the present samples (Table 1) may be due to the presence of water or hydroxyl groups within the films, which typically occur for amorphous structures. At higher substrate temperatures of 300 and 400°C, the crystalline films possess lower stoichiometry. Moreover, a sodium peak tends to appear in the spectra for the films deposited at higher temperatures. The presence of sodium in the films indicates that diffusion of Na atoms from the soda lime glass substrate occurs at higher substrate temperatures. Blackman and Parkin[11] reported overstoichiometric monoclinic tungsten oxide (atomic ratio, 3·3) prepared on SiCO coated soda lime glass substrate by APCVD. Sivakumar *et al.*[30] also reported atomic concentrations for monoclinic tungsten oxide films deposited at different temperatures on fluorine doped tin oxide coated glass substrates using X-ray photoelectron spectroscopy spectral analysis. They found higher atomic ratio (O/W) of 3·72 for the film deposited at room temperature. The effects of substrate temperatures on ratios of O/W (at-%) are nearly comparable to the present work. In this present research, overstoichiometric WO_3 films are also thought to be due to the higher oxygen content inside the vacuum chamber.

Surface morphologies of the as grown WO_3 films at different substrate temperature are shown in Fig. 2. The film prepared at room temperature exhibits a relatively flat topography. A careful look at the film reveals network of minute crack-like features. The cracks tend to disappear as the substrate temperature increases. The morphology also becomes granular as the substrate temperature increases. The size of the granular features also increases with the increase in substrate temperature. The size of the granules is found to be in the range of 10–50 nm for the film deposited at 300°C (Fig. 2*c*). The film deposited at 400°C shows larger granules of 20–80 nm. Blackman and Parkin[11] reported a granular morphology for WO_3 film deposited at 450°C on glass substrates using atmospheric pressure chemical vapour deposition. The cross-sectional views of the WO_3 film deposited at different temperatures are shown in Fig. 3. Under an SEM, the film thicknesses are observed to be about 335, 420, 420 and 425 nm for the films deposited at room temperature and at 200, 300 and 400°C respectively. The cross-sectional morphology for the films grown at room temperature and 400°C tends to be granular in nature and possesses more or less dense structure. However the film deposited at 200°C exhibits a columnar cross-sectional morphology. Besides, both films deposited at lower temperatures seem to have either transverse or vertical cracks. Such fine cracks were also found on plane views of the films deposited at lower temperatures (Fig. 2*a* and *b*). Both plane and cross-sectional views (Figs. 2*d* and 3*c*) of the films deposited at 400°C show that the film possesses dense and granular morphology without any distinct cracks. Figueroa *et al.*[17] observed columnar structure in their WO_3 films deposited on indium tin oxide coated glass by rf reactive magnetron sputtering. They prepared the films at a sputtering pressure of ~0·5 Pa, which is lower compared to the present work.

Adhesion behaviour

The adhesion critical load of the studied tungsten oxide films was determined by the microscratch tests combined with the observation of the scratch tracks under the optical microscope. Three different microscratch tests were performed on the as received blank glass at room temperature. Triplicate tests were also carried out on each of the tungsten oxide films. Tests carried out in triplicate gave consistent results. Optical micrographs of the scratch scars are shown in Fig. 4. It is observed that the width of each scratch track increases as the load is progressively increased. At a certain point (shown by arrows), a widely damaged area appears representing a complete delamination of the films, which can be defined as the critical load for adhesion. Two types of failure are mainly encountered in scratch tests, namely, cohesive and adhesive failures of the coating/substrate interface.[29] The former occurs having a narrow region of slightly damaged films, and then the film remains undamaged. On the other hand, for the adhesive or interfacial failure, the complete delamination of the films starts and continues for the rest of the scratch track. The cohesive values are difficult to quantify because either coatings do not exhibit such failure or the values are very close to the adhesive ones. From Fig. 4, it is observed that no significant cohesive failure mode appears and adhesive critical load is found as larger for the films deposited at a higher temperature up to 300°C. However the film prepared at 400°C exhibits earlier damages indicating cohesive failures. Moreover, it also shows earlier adhesive failure compared to the other films. The critical

Table 1 EDX results of WO_3 films deposited at different substrate temperatures

Substrate temperature/°C	Concentration/at-%			Atomic ratio
	W	O	Na	O/W
Room temperature	21·92	78·08	0	3·56
200	21·41	78·26	0·33	3·65
300	23·38	75·34	1·28	3·22
400	22·13	74·55	3·32	3·37

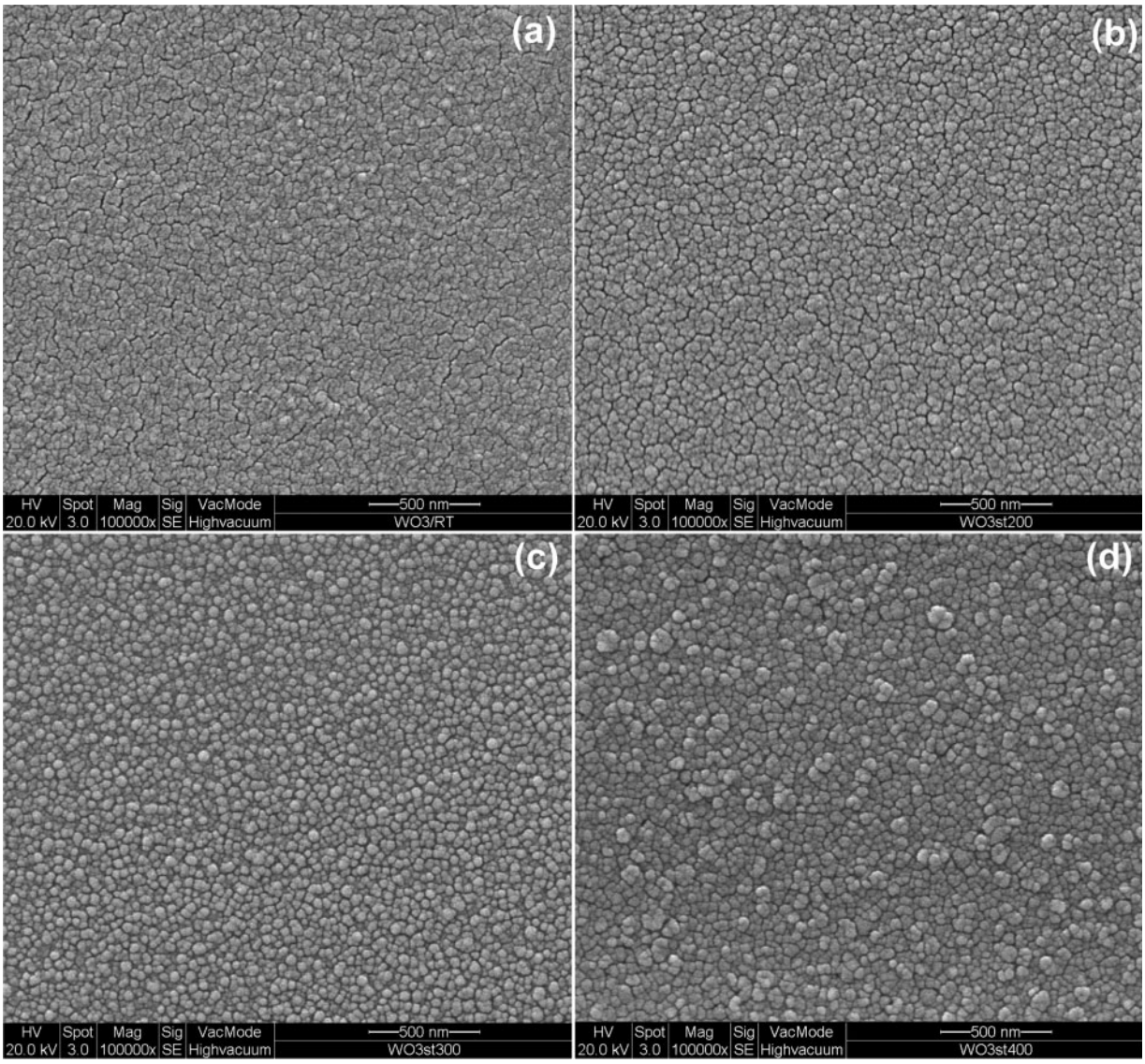

2 Images (SEM) of WO_3 films deposited at *a* room temperature, *b* 200°C, *c* 300°C and *d* 400°C

loads of the films deposited at room temperature and at 200, 300 and 400°C were estimated from the scratch curves and found to be 670, 990, 1080 and 830 mN respectively. It is thus seen that the increase in substrate temperatures up to 300°C leads to improved adhesion of tungsten oxide films on glass substrates. There are suggestions that interdiffusion of film/substrate interface can cause enhanced film adhesion.[31] The increase in adhesion critical load may be due to interdiffusion of atoms in the film/substrate interface and densification of the films at higher substrate temperatures up to 300°C. The lower critical load for the film grown at 400°C may be attributed to a clear change in coating structure, composition and morphology (Table 1 and Fig. 2). Besides, there was a significant amount of Na atom incorporation into the film (Table 1) as well. At higher substrate temperatures, Na is thought to diffuse from glass substrates to the films. Higher residual stress resulting from mismatch of coefficients of thermal expansion of the substrate and films deposited at 400°C might also contribute to this.

Parreira *et al.*[15] reported a critical load of ~15 N for tungsten oxide films (2·5–6 μm thick) deposited on stainless steel at 350°C by dc magnetron sputtering. Polcar and Cavaleiro[16] also reported a critical load of 9 N for WO_3 films having similar thickness deposited by dc magnetron sputtering on high speed steel. Both works evaluated critical loads by the scratch tests using a diamond indenter of tip radius 200 μm. In the present study, a spherical diamond indenter tip of radius 25 μm was used to generate scratch on thin WO_3 films (335–425 nm thick) during microscratch tests. The smaller radius of the indenter tip used in this study produces a high contact pressure on the films. This is likely to be a reason for the coating failures at lower values of critical loads in the present investigation. There are suggestions that critical load increases with the increase in film thickness.[29] As a result, it can be inferred that the lower values of critical loads obtained in this work may be attributed to the combined effects of nanoscale film thickness, indenter tip radius, substrate materials and coating/substrate interfaces.

Scratch hardness

The values of scratch hardness are calculated using equation (2). The scratch hardness and critical loads are given in Table 2. From the table, the values of scratch

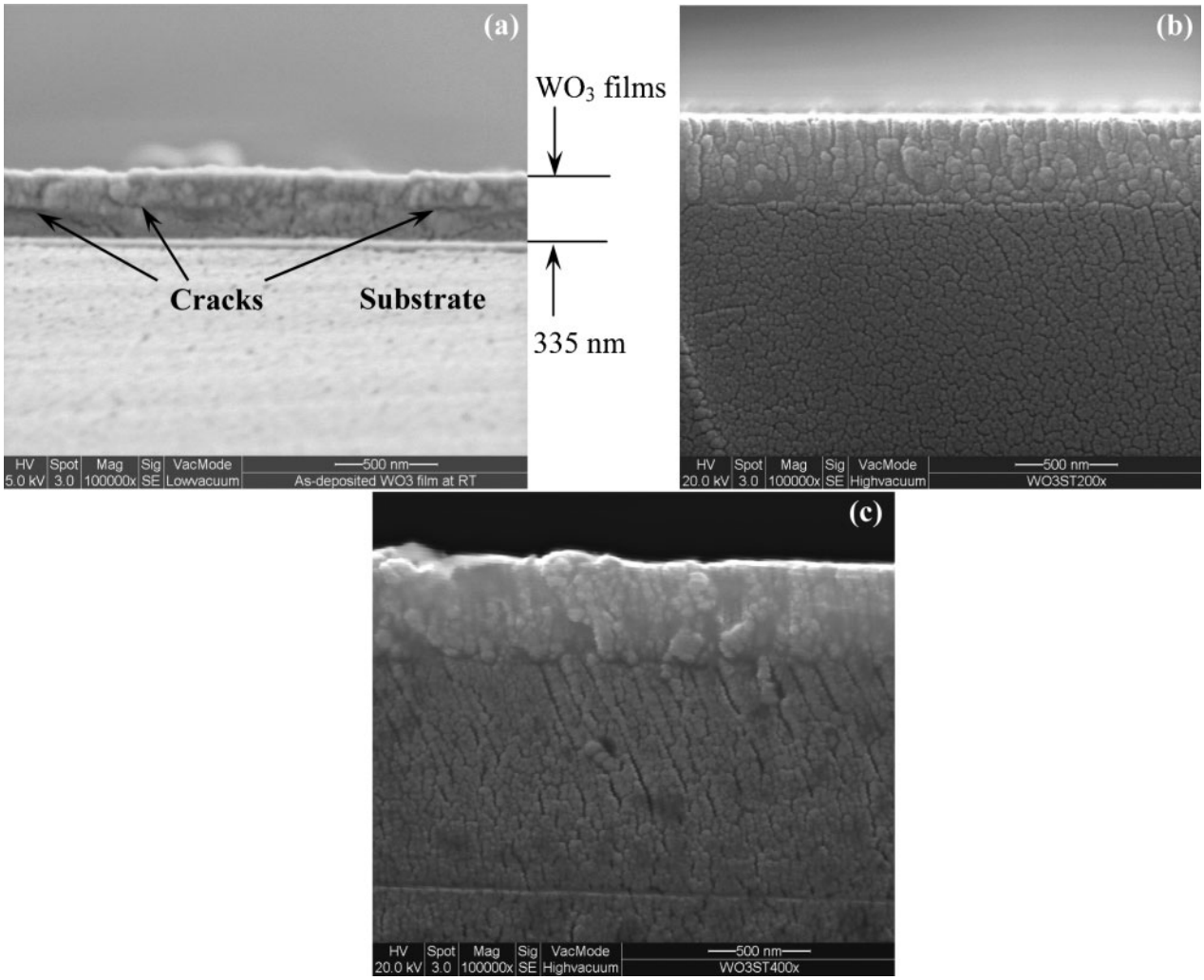

3 Cross-sectional views (SEM) of WO_3 films deposited at *a* room temperature, *b* 200°C and *c* 400°C

hardness are found to be 10·8, 15·2, 16 and 19·5 GPa for WO_3 films prepared at room temperature and at 200, 300 and 400°C respectively. Because of the nanoscale thickness of the films, it is likely that the substrate also contributes to the measurements of scratch hardness. In addition, the values might be exaggerated due to the evenly supported sliding probe during microscratch tests as well as the errors associated with the scratch width values estimated using optical microscopy. However, scratch hardness is found to increase with the increase in substrate temperatures. Table 2 shows that the critical load and scratch hardness values have the same increasing trend except for the film grown at 400°C. Particularly, the sudden decrease in critical load for that

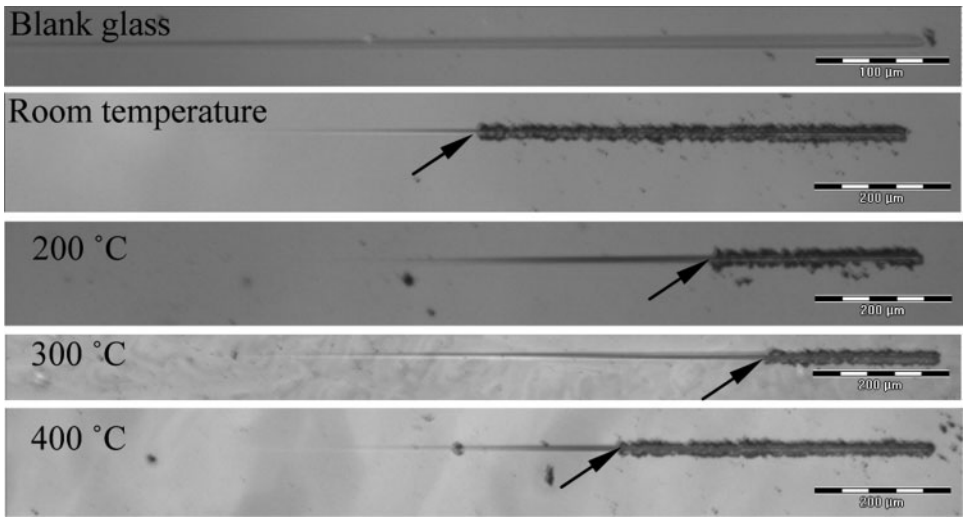

4 Optical micrographs of scratches made under progressively increasing load on blank glass and WO_3 films deposited at different temperatures

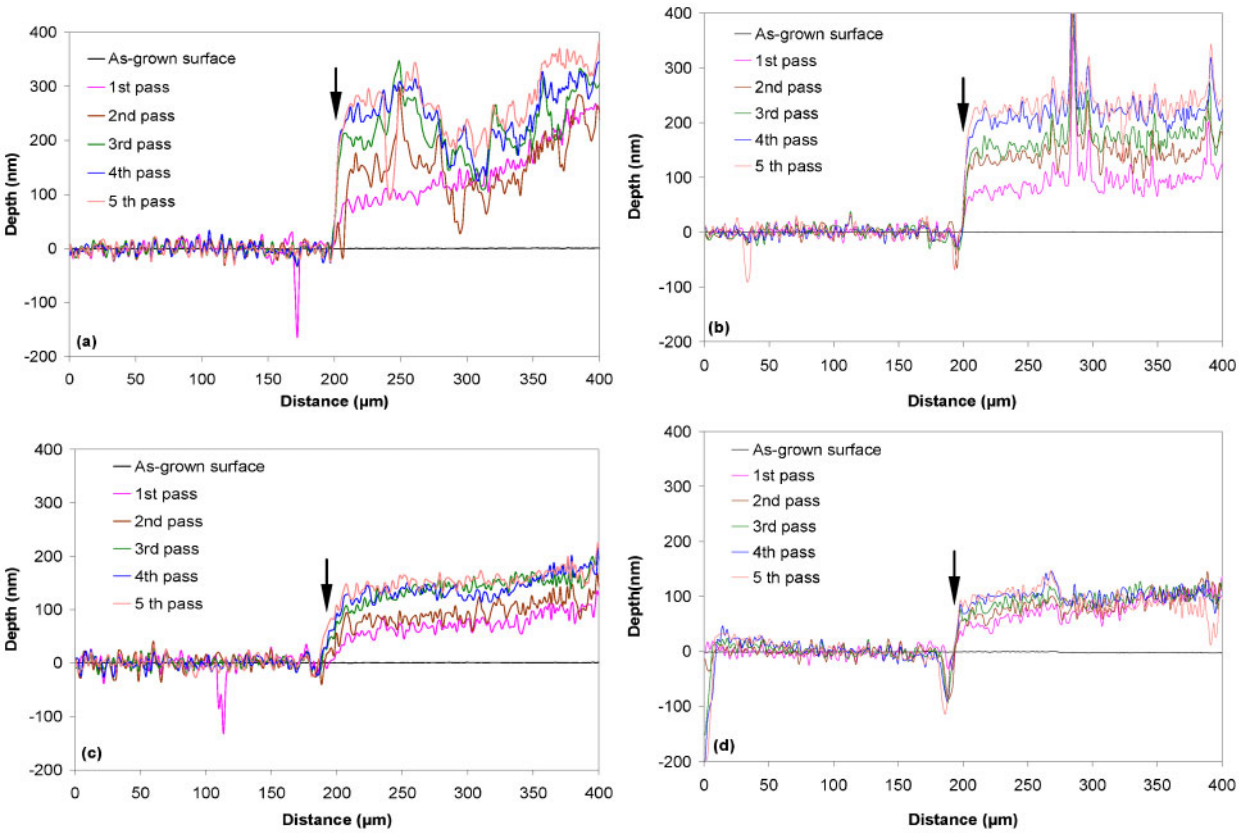

5 Wear tests for WO_3 films deposited at *a* room temperature, *b* 200°C, *c* 300°C and *d* 400°C

sample may be due to the effects of significant Na diffusion and higher residual stress. Parreira *et al.*[15] and Polcar and Cavaleiro[16] reported a decrease in surface hardness from 25 to 7 GPa with the increase in oxygen content for $W_{100-x}O_x$ films (determined by nanoindentation) of 2·5–6 μm thick. They both found a hardness of ~7 GPa for WO_3 films having amorphous phase. Maillé *et al.*[13] reported hardness of 4 GPa for amorphous tungsten oxide film (350 nm) deposited on silicon substrates by rf magnetron sputtering. The scratch hardness values found in the present study are nearly comparable to the surface hardness values found in those studies. Besides, Lugscheider *et al.*[27] observed a decrease in hardness from 28 to 13 GPa for tungsten oxide films as substrate temperature increases. In that work, the films investigated were XRD amorphous with different stoichiometries.

Tribological properties

In tribological tests, a spherical diamond indenter of radius 25 μm of NanoTest high load head equipment is drawn unidirectionally along the same surface using a load of 500 mN at a sliding speed of 1 μm s^{-1} for a wear track distance of 800 μm. Figure 5 shows the surface profiles recorded after five successive wear passes. The surface profiles of the as grown films are also shown for comparison. Data extracted from Fig. 5 are plotted in Fig. 6 as penetration depth versus substrate temperature. Here, any value for the total penetration depth has been considered as the vertical distance moved by the diamond probe at the point of loading (indicated by arrow in Fig. 5) with respect to the as grown film surface. It is observed that upon the application of load, the penetration depth suddenly increases. From Fig. 6, it is seen that the films deposited at higher substrate temperatures exhibit lower penetration. Thus, higher deposition temperature results in tungsten oxide film with improved resistance to penetration. This result correlates well with the increase in scratch hardness for higher substrate temperatures as discussed earlier. Noteworthy, the change in wear tracks of the films is thought to occur by the combined effects of wear and initial plastic deformation. Figure 7 presents FESEM images of the wear tracks after five passes on films deposited at room temperature and at 200 and 400°C. From the SEM images in Fig. 7, the wear debris and delaminated films along the side of the wear tracks are also observed for all the films. From the FESEM images at a high magnification ($\times$280 and $\times$4000), it is seen that wear resistance improves with the increase in

Table 2 Scratch hardness, adhesion critical load and wear track width of WO_3 films deposited at different substrate temperatures

Substrate temperature/°C	Film thickness/nm	Critical load/mN	Scratch hardness/GPa	Mean wear track width/μm
Room temperature	335	670	10·8	22·3
200	420	990	15·2	17·4
300	420	1080	16·0	10·9
400	425	830	19·5	10·4

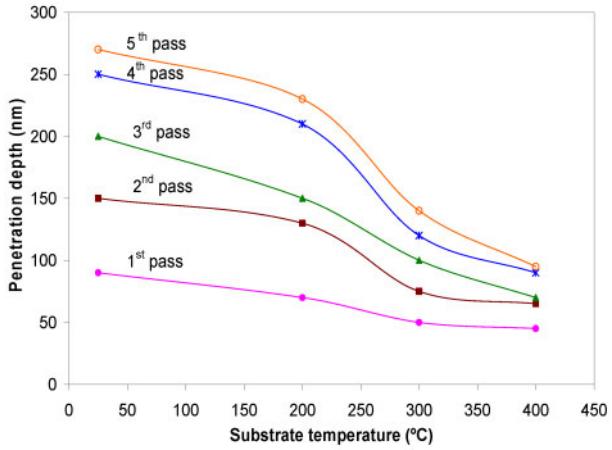

6 Total depth of penetration after each wear pass for WO_3 films deposited at different temperatures

substrate temperature up to 300°C. However, the film deposited at 400°C shows deterioration of wear resistance. This is supported by the lower value of adhesion critical load observed (Table 2). It may also be attributed to its structural and morphological change as stated earlier. From the SEM images, it is also seen that amount of wear debris is smaller for the films at higher substrate temperature except for the sample grown at 400°C.

The mean width of the wear tracks of WO_3 films deposited at different substrate temperatures is given in Table 2. It is observed that the width of the wear track is found to decrease with increasing substrate temperature, which is consistent with the penetration data. Thus, it can be inferred that wear resistance is found to improve at higher substrate temperatures (up to 300°C). The change in the tribological properties may be interpreted as the effects of adhesion strength at different substrate temperatures as well. Moreover, amorphous tungsten oxide films show higher amount of wear than crystalline films. In this regard, Greenwood *et al.*[25] and Lugscheider *et al.*[26] observed that amorphous WO_3 films exhibited a higher degree of wear compared to crystalline films. Polcar *et al.*[14] also reported that abrasive wear for amorphous $W_{100-x}O_x$ (15–75 at-%) films having higher oxygen (x) contents is found higher than that of crystalline films with lower oxygen contents. The similar trend of wear is nearly comparable to the studied films of different stoichiometry. In the present work, the change of wear resistance may be attributed to the total contribution from the change in crystallinity, critical load, scratch hardness and sodium ion diffusion for films deposited at higher substrate temperatures.

Coating failures

The failure modes in the scratch testing of coatings can broadly be split into three categories: through thickness cracking, spallation ahead or behind the indenter and chipping in the coating.[32–34] From the optical micrographs (Fig. 4), it seems that all as grown films have similar failure mode during scratch tests. That is why SEM images for the tungsten oxide films grown at room temperature and at 400°C have been shown in Fig. 8 to depict the mode of coating failures. From Fig. 8, the failure modes encountered in both films during scratch test can be considered as wedge spallation in front of the indenter. The wedge spallation failure mode occurs only when a compressive shear crack forms and then interfacial detachment takes place.[35] First, compressive shear cracks form ahead of the indenter through the thickness, which propagate to the surface and interface generating shapes like a wedge. As the extent of interfacial failure increases, the wedge lifts the coating

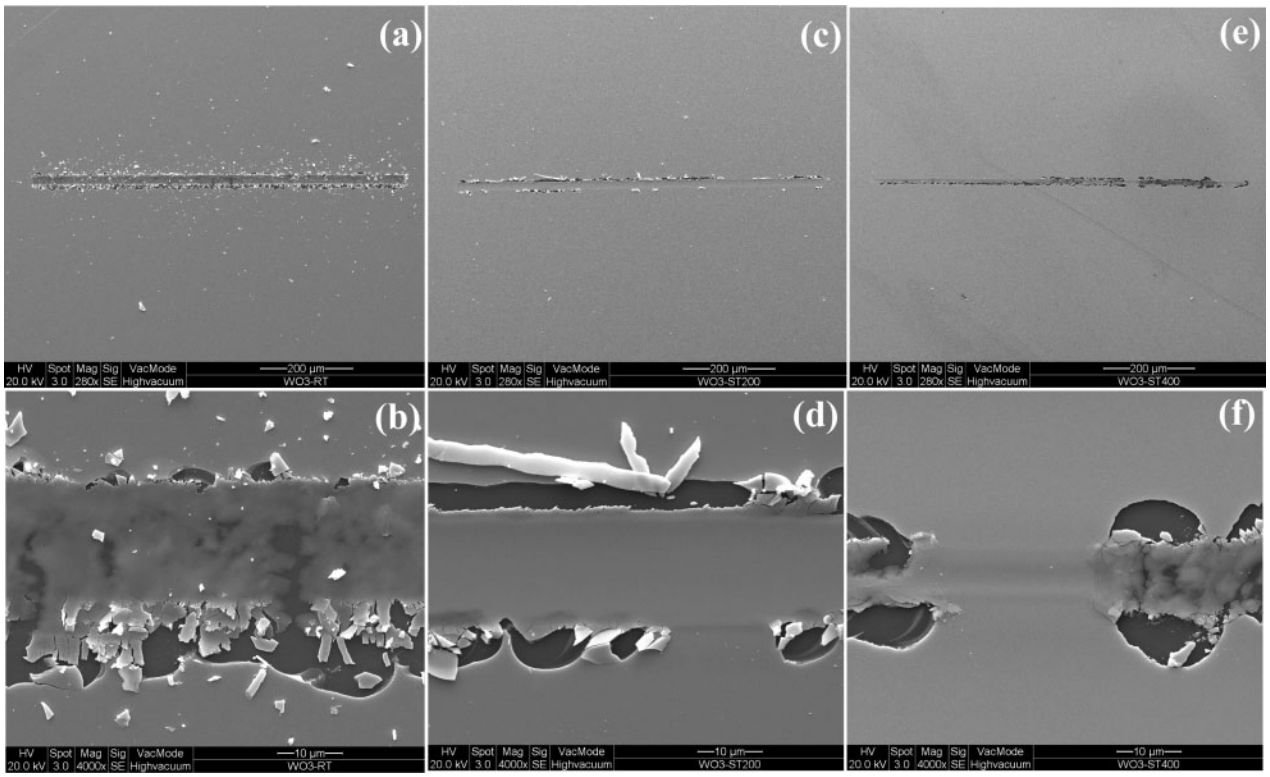

7 Image (SEM) of wear scars on WO_3 films deposited at *a*, *b* room temperature, *c*, *d* 200°C and *e*, *f* 400°C after five passes

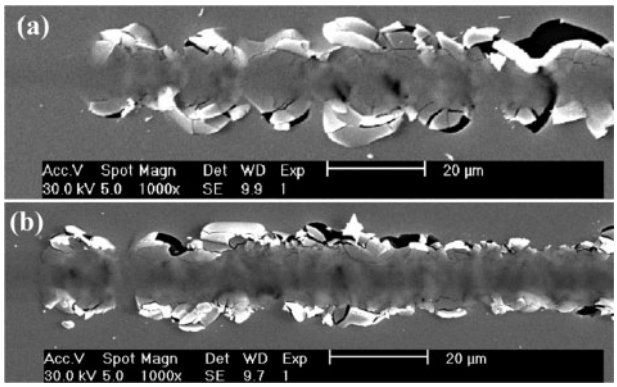

8 Images (SEM) for scratches on WO_3 films deposited at *a* room temperature and *b* 400°C (×1000)

further away from the substrate. In wear tests, all the as received films are also found to fail along the edge of the wear tracks as shown in Fig. 7. The failure modes encountered in the studied films during wear tests can be considered as recovery spallation behind the indenter. It is associated with the elastic recovery, which occurs behind the stylus as it travels over the coated surface.

Conclusion

Mechanical properties along with structural and morphological properties of WO_3 films deposited at different temperatures have been studied in details. The films deposited at lower temperature are found as amorphous, whereas the films at 300 and 400°C exhibit a mixed monoclinic and orthorhombic phase having nanograins of 9 and 13·5 nm respectively. The overstoichiometry of the films may be due to the presence of water or hydroxyl groups. Energy dispersive X-ray results reveal that the diffusion of sodium ions from glass substrates occurs for high deposition temperatures. The adhesion critical load, scratch hardness and wear resistance are seen to have significant dependence on the substrate temperature. The critical loads of adhesion of WO_3 films grown at room temperature and at 200, 300 and 400°C are found to be 670, 990, 1080 and 830 mN respectively. The values of scratch hardness are also found to increase with the increase in substrate temperatures. From wear tests, the combined decrease in penetration and wear track width results in an enhanced wear resistance for the films deposited at higher temperatures. This improvement of wear properties is likely to be attributed to the improved scratch hardness, densification and compositional change. The failure modes of wedge and recovery spallation have been observed for the films during scratch and wear tests respectively.

Acknowledgements

The authors gratefully acknowledge the financial support given for this work by the Ministry of Science, Technology and Innovation Malaysia (MOSTI) under the ScienceFund by grant no. 13-02-03-3033 and the Institute of Research Management and Consultancy, University of Malaya (UM) by PPP Fund project no. PS 380/2008C. The authors also pay thanks to Dr M. Hamdi, Professor, Department of Engineering Design and Manufacturing, UM, for allowing us to use his vital research facilities.

References

1. C. G. Granqvist, S. Green, G. A. Niklasson, N. R. Mlyuka, S. von Kræmer and P. Georén: *Thin Solid Films*, 2010, **518**, 3046–3053.
2. J. Zhang, X. L. Wang, X. H. Xia, C. D. Gu and J. P. Tu: *Sol. Energy Mater. Sol. Cells*, 2011, **95**, 2107–2112.
3. M. Giannouli and G. Leftheriotis: *Sol. Energy Mater. Sol. Cells*, 2011, **95**, 1932–1939.
4. H.-H. Lu: *J. Alloys Compd*, 2008, **465**, 429–435.
5. I. Valyukh, S. Green, H. Arwin, G. A. Niklasson, E. Wäckelgård and C. G. Granqvist: *Sol. Energy Mater. Sol. Cells*, 2010, **94**, 724–732.
6. X. Sun, H. Cao, Z. Liu and J. Li: *Appl. Surf. Sci.*, 2009, **255**, 8629–8633.
7. C. Zhang, M. Debliquy, A. Boudiba, H. Liao and C. Coddet: *Sens. Actuators B*, 2010, **144B**, 280–288.
8. Y. Shen, T. Yamazaki, Z. Liu, D. Meng, T. Kikuta and N. Nakatani: *Thin Solid Films*, 2009, **17**, 2069–2072.
9. C. Gu, J. Zhang and J. Tu: *J. Colloid Interface Sci.*, 2010, **352**, (2), 573–579.
10. S. Yamamoto, A. Inouye and M. Yoshikawa: *Nucl. Instrum. Methods Phys. Res. B*, 2008, **266B**, 802–806.
11. C. S. Blackman and I. P. Parkin: *Chem. Mater.*, 2005, **17**, 1583–1590.
12. M. F. Al-Kuhaili, A. H. Al-Aswad, S. M. A. Durrani and I. A. Bakhtiari: *Sol. Energy*, 2009, **83**, 1571–1577.
13. L. Maillé, C. Sant, P. Aubert and P. Garnier: *Thin Solid Films*, 2005, **479**, 201–206.
14. T. Polcar, N. M. G. Parreira and A. Cavaleiro: *Vacuum*, 2007, **81**, 1426–1429.
15. N. M. G. Parreira, N. J. M. Carvalho and A. Cavaleiro: *Thin Solid Films*, 2006, **510**, 191–196.
16. T. Polcar and A. Cavaleiro: *Int. J. Refract. Met. Hard Mater.*, 2010, **28**, 15–22.
17. R. Figueroa, M. Kleinke, Tersio G. S. Cruz and A. Gorenstein: *J. Power Sources*, 2006, **162**, 1351–1356.
18. A. A. Akl, H. Kamal and K. Abdel-Hady: *Physica B*, 2003, **325B**, 65–75.
19. H. Wang, P. Xu and T. Wang: *Mater. Des.*, 2002, **23**, 331–336.
20. D. Işık, M. Ak and C. Durucan: *Thin Solid Films*, 2009, **518**, 104–111.
21. S. Balaji, Y. Djaoued, A. S. Albert, R. Bruning, N. Beaudoinc and J. Robichaud: *J. Mater. Chem.*, 2011, **21**, 3940–3948.
22. Z. Dimitrova and D. Gogova: *Mater. Res. Bull.*, 2005, **40**, 333–340.
23. F. Chávez, C. Felipe, E. Lima, V. Lara, C. Ángeles-Chávez and M. A. Hernandez: *Mater. Chem. Phys.*, 2010, **120**, 36–41.
24. R. Sivakumar, K. Shanthakumari, A. Thayumanavan, M. Jayachandran and C. Sanjeeviraja: *Surf. Eng.*, 2007, **23**, (5), 373–379.
25. O. D. Greenwood, S. C. Moulzolf, P. J. Blau and R. J. Lad: *Wear*, 1999, **232**, 84–90.
26. E. Lugscheider, O. Knotek, K. Bobzin and S. Bärwulf: *Surf. Coat. Technol.*, 2000, **133/134**, 362–368.
27. E. Lugscheider, S. Bärwulf and C. Barimani: *Surf. Coat. Technol.*, 1999, **120/121**, 458–464.
28. B. D. Cullity: 'Elements of X-ray diffraction', 2nd edn, 102; 1978, London, Addison-Wesley.
29. J. Malzbender, J. M. J. den Toonder, A. R. Balkenende and G. de With: *Mater. Sci. Eng. R*, 2002, **R36**, 47–107.
30. R. Sivakumar, R. Gopalakrishnan, M. Jayachandran and C. Sanjeeviraja: *Smart Mater. Struct.*, 2006, **15**, 877–888.
31. C. J. Chung, P. Y. Hsieh, C. H. Hsiao, H. I. Lin, A. Leyland, A. Matthews and J. L. He: *Surf. Coat. Technol.*, 2009, **203**, 1689–1693.
32. S. J. Bull: *Tribology Int.*, 1997, **30**, (7), 491–498.
33. F. Yıldız, A. Alsaran, A. Celik and I. Efeoglu: *Surf. Eng.*, 2010, **26**, (8), 578–583.
34. E. Arslan, Y. Totik, A. Celik and I. Efeoglu: *Surf. Eng.*, 2010, **26**, (8), 567–570.
35. S. J. Bull and E. G. Berasetegui: *Tribology Int.*, 2006, **39**, 99–114.